Research Article Adv. Mat. Lett. 2013, **4**(4), 288-295 ADVANCED MATERIALS Letters

www.amlett.com, www.amlett.org, DOI: 10.5185/amlett.2012.8416

Synthesis, electrical and dielectrical properties of lithium iron oxide

P. Rosaiah, O. M. Hussain[*]

Thin film Laboratory, Department of Physics, Sri Venkateswara University, Tirupati 517 502, India

[*]Corresponding author. E-mail: hussainsvu@gmail.com

Received: 31 August 2012, Revised: 16 October 2012 and Accepted: 10 November 2012

ABSTRACT

Lithium iron oxide ($LiFeO_2$) cathode material was prepared by using hydrothermal synthesis. The XRD spectrum exhibited predominant (200) orientation peak at $2\theta = 43.63^o$ corresponding to cubic rock-salt structure with Fm3m space group and the estimated lattice parameter of the sample is 4.176 Å. Electric and dielectric properties were studied over a frequency range of 1 Hz – 1 MHz and in the temperature range from 300 K to 573 K. The ionic conductivity of the sample was found to be 1.9×10^{-6} S/m at 373 K. The temperature dependent conductivity was conformed from the Arrhenius relation and the activation energy was found to be 0.39 eV. A mixed, ionic and electronic conduction was observed from the analysis. The electrical conductivity was found to be decreased with increasing temperature. The dielectric properties were analyzed in the framework of complex dielectric permittivity and complex electric modulus formalisms. The evolution of the complex permittivity as a function of frequency and temperature was investigated. Several important parameters such as activation energy, ionic hopping frequency, carrier concentration, ionic mobility and diffusion coefficient etc, were determined. Copyright © 2013 VBRI press.

Keywords: Hydrothermal synthesis; $LiFeO_2$ cathode material; electrical and dielectric analysis.

P. Rosaiah was born in 1984. He received M.Sc. and M.Phil. in Physics from Sri Venkateswara University, Tirupati, India in 2007 and 2010. He is pursuing Ph.D. in the field of thin films. He has published 3 papers in refereed journals. He has presented more than 10 papers in National/International conferences. He is currently working in the area of metal oxide thin film cathodes for micro-battery applications.

O. M. Hussain has received M.Sc. and Ph.D. degrees in Physics from Sri Venkateswara University, Tirupati, India in 1984 and 1990. Later, he worked as Post Doctoral Fellow during 1991-92 in Universite Pierre et Marie Curie, Paris, France. He joined as a faculty member in 1992 in the Department of Physics, S.V.University and currently working as a professor. His research interests are growth of poly crystalline and nanocrystalline metal oxide thin films for electrochemical, electrochromic and gas sensor applications. So far, he has guided 09 Ph.D. students and 07 M.Phil. students and published about 115 research articles in peer reviewed journals. He has successfully completed several major research projects funded by University Grants Commission (UGC), Department of Science and Technology (DST), Defense Research Development Organization (DRDO) etc.

Introduction

Lithium ion batteries have become the dominant power sources for portable electronic devices because of their high energy density. Many researchers have investigated different cathode materials for the lithium secondary batteries such as layered oxides, $LiMO_2$ (M: Co, Ni, Mn, Fe) [**1-4**]. Layered lithium metal oxide materials have rock-salt structure where lithium and transition metal ion occupying alternate layer of octahedral sites in a distorted close-packed oxygen ion lattice. $LiCoO_2$ has been most widely used cathode material in commercial lithium ion batteries. But, It has many problems such as high toxic, high cost, low practical capacity etc [**5-6**]. Therefore alternate cathode materials with low cost and non toxicity have been studied in recent years. Among lithium transition metal oxides, $LiFeO_2$ with similar rock-salt structure to $LiCoO_2$, has been paid more attention due to most abundance and non-toxicity of iron. In recent years, great progress has been made recently on its preparation, structure and modification due to extensive use of new synthesis methods [**7**].

$LiFeO_2$ has various crystalline structures such as α-$LiFeO_2$, β-$LiFeO_2$, γ-$LiFeO_2$, Layered $LiFeO_2$, Corrugated $LiFeO_2$, Goethite type $LiFeO_2$ etc [**8-9**]. The crystalline structure of $LiFeO_2$ depends mainly on the preparation methods. Many researches prepared $LiFeO_2$ with different structures. V.R. Galakhov et al. prepared α-$LiFeO_2$ with

Fm-3m space group by using solid state reaction and M. Tabuchi et al. prepared α-$LiFeO_2$ with Fm3m space group by hydrothermal synthesis [**10**]. Similarly, β-$LiFeO_2$, γ-$LiFeO_2$ and layered $LiFeO_2$ are prepared by hydrothermal synthesis and other methods [**11-12**]. Corrugated $LiFeO_2$ and Goethite type $LiFeO_2$ are prepared by ion exchange method [**13**]. In comparison with the conventional solid-phase synthesis methods [**14**], hydrothermal method is one of the simplest and best methods to prepare lithium based cathode materials. The hydrothermal process is a relatively low temperature process and has many advantages such as fast reaction kinetics, short processing times, high crystallinity, high yield, cost effective and environmentally benign. Also, complex oxide materials with phase purity along with controlled and homogeneous particle sizes can be achieved by properly controlling the process parameters. Hence, in the present investigation α-$LiFeO_2$ was prepared by using hydrothermal synthesis.

Studies on the conductivity of lithiated cathode materials are important in order to gain a better imminent on the ionic conduction mechanism especially in its usage for lithium-ion batteries. Dielectric and impedance spectroscopy is widely used for investigating the electrical and electrochemical properties [**15**]. The application of ac technique of complex impedance analysis is important and eliminates pseudo effects if any in the material. Complex impedance analysis makes it possible to separate the contribution due to grain, grain boundary and interfacial effects. Generally, these properties depend on the resistive and capacitive components in the material. So that, the result obtained from these analyses provide true representation of electrical behavior of the sample. In case of the electrical properties of the oxides, grain boundaries play an important role. The measurement of conductivity and permittivity shows dispersion behavior which offers an opportunity to gain some information of ionic migration process. Considering the significance, the electrical conductivity studies on various lithium-based oxides such as $LiCoO_2$, $LiCeO_2$, $LiSmO_2$, Li_2SnO_3, Li_2MnO_3, $LiMn_2O_4$, and $Li_2V_2O_5$, and others have been reported in the literature [**16-19**]. However, to the best of our knowledge, there are meager reports on electrical and dielectric properties of $LiFeO_2$. A detailed study on the temperature and frequency depended electrical properties is necessary to understand the conduction mechanism in $LiFeO_2$ for effective utilization as cathode material in the fabrication of lithium ion batteries. Hence, in the present study, α-$LiFeO_2$ nanocrystalline powder is synthesized from hydrothermal process and systematically characterized. The main emphasis has been focused on the study of electrical conduction mechanism and dielectric behavior. From the conductivity studies, various important parameters such as activation energy, ionic hopping frequency, carrier concentration, ionic mobility, diffusion coefficient etc. are estimated and the results are discussed.

Experimental

α-$LiFeO_2$ with Fm3m space group was prepared by using hydrothermal synthesis. For that, α-FOOH, Kanto Chemical Co., (High purity) and $LiOH.H_2O$, Aldrich (98% purity) were used as initial materials. To prepare α-$LiFeO_2$, α-FOOH was mixed with $LiOH.H_2O$ in distilled water (Li/Fe molar ratio = 30) using a Teflon beaker to avoid reaction with the vessel. The mixture was treated hydrothermally at 250 ^{o}C and 25 Kgf/cm^2 for 6 h. The product washed repeatedly with distilled water to eliminate residual $LiOH.H_2O$ and dried at 100^{o}C for long time. The prepared powder was pressed into 12 mm diameter pellet with the thickness of 1 mm and then annealed at 500 ^{o}C for 5 h to eliminate impurity phases, if any and to enhance the crystallinity of the sample.

The structure of the prepared sample is studied by the X-ray diffraction technique (Siefert computerized X-ray diffractometer, model 3003 TT) using Cu$K_{\alpha 1}$ radiation (λ=0.15406 nm) source filtered by Ni thin film at a scan speed of 0.05 degree per second in the 2θ □range 15 – 50 ^{o} and operated at a voltage of 40 KV and a current 30 mA. The peak positions are determined precisely using RAYFLEX-Analyze software. The particle size and shape was observed by Scanning electron microscope (SEM, HITACHI, Model: S-3400N) operated in High Vacuum mode. The Composition of the sample is analyzed by EDAX system (Oxford Instruments, UK). The impedance measurements were performed using a Phase Sensitive Multimeter (Model: PSM 1700, UK) in the range of 1 Hz to 1 MHz at different temperatures ranging from room temperature to 573 K. The measurements were made on a pressed sintered $LiFeO_2$ pellets coated on both sides with gold paste in a controlled environment. The data was corrected for sample geometry (area/thickness) prior to analysis, the parallel capacitance of the jig and series resistance of the leads and electrodes. The experimental data in real and imaginary part of the formulism Z, M and ϵ versus frequency at different temperatures are recorded.

Electrical and dielectric calculations

The electrical parameters such as impedance Z, real part of the dielectric permittivity ε', imaginary part of dielectric permittivity or dielectric loss ε'' ac conductivity σ_{ac} were measured by using Phase Sensitive LCR meter. The dielectric constant ε', and dielectric loss ε'' of $LiFeO_2$ sample were calculated by using following relationship.

$$\text{Dielectric constant } (\varepsilon') = ct/\varepsilon_o A \qquad (1)$$

$$\text{Dielectric loss } (\varepsilon'') = \sigma_{ac}/\varepsilon_o \omega \qquad (2)$$

where 't' is thickness of the pellet, 'A' is the cross sectional area of the sample, ε_o is the permittivity of the free space and σ_{ac} is the ac conductivity of the sample.

The ac conductivity is calculated by using conductance (G) as follows:

$$\text{ac conductivity } (\sigma_{ac}) = tG/A \qquad (3)$$

The values of ε' and ε'' were used to determine the loss tangent (tan δ) using following expression:

$$\varepsilon'' = \varepsilon' \tan \delta \qquad (4)$$

where δ is the phase angle between the electric field and the polarization of the dielectric.

The calculated values of the ε’ and ε’’ were used to calculate the real part (M’) and imaginary part (M”) of the electric modulus as follows:

$$M' = \varepsilon'/(\varepsilon'^2 + \varepsilon''^2) \quad (5)$$

$$M'' = \varepsilon''/(\varepsilon'^2 + \varepsilon''^2) \quad (6)$$

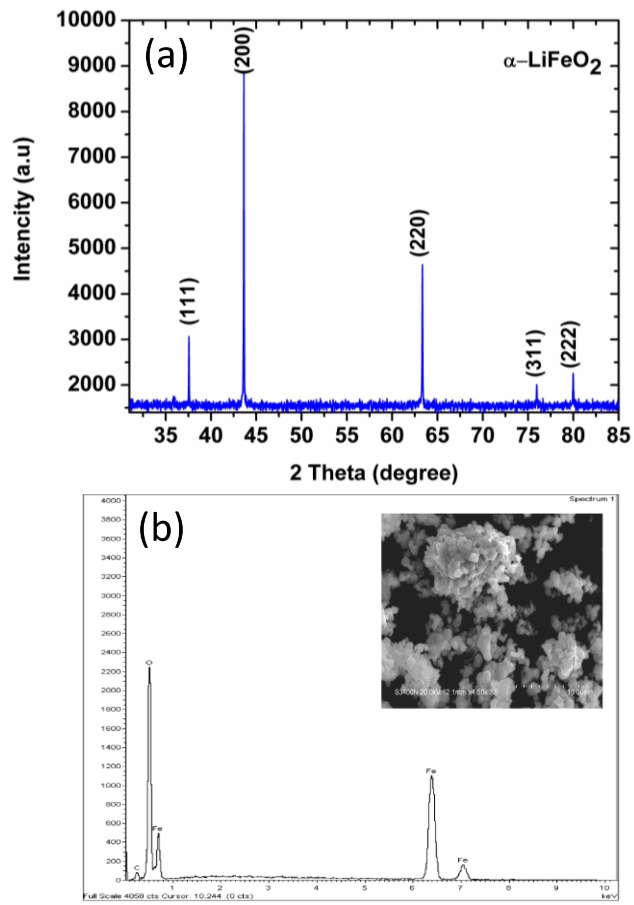

Fig. 1. (a) X-ray diffraction and (b) EDAX spectra of $LiFeO_2$. Inset figure shows the SEM image.

Results and discussion

Structural analysis

Fig. 1 (a) shows the XRD pattern of $LiFeO_2$ sample. All the diffraction peaks were indexed with α-$LiFeO_2$. The XRD spectrum exhibited predominant peak (200) orientation at $2\theta = 43.63^o$ along with other characteristic orientations (110), (220), (311), (222) at 37.56^o, 63.34^o, 75.95^o and 80.00^o respectively corresponding to cubic rock-salt structure with Fm3m space group. The estimated lattice parameter of the sample is 4.176 Å [**20**]. The crystallite size of the prepared sample was estimated using Debye-Scherrer formula:

$$L = K \times \lambda / \beta \times \cos\theta$$

where β is the full width half maximum (FWHM) in radians, λ is the wavelength of the X-ray, θ is the corresponding Bragg angle and K is the constant (k=0.9). The estimated crystallite size is about 60 nm. The EDAX experiments were used for the chemical analysis of the sample.

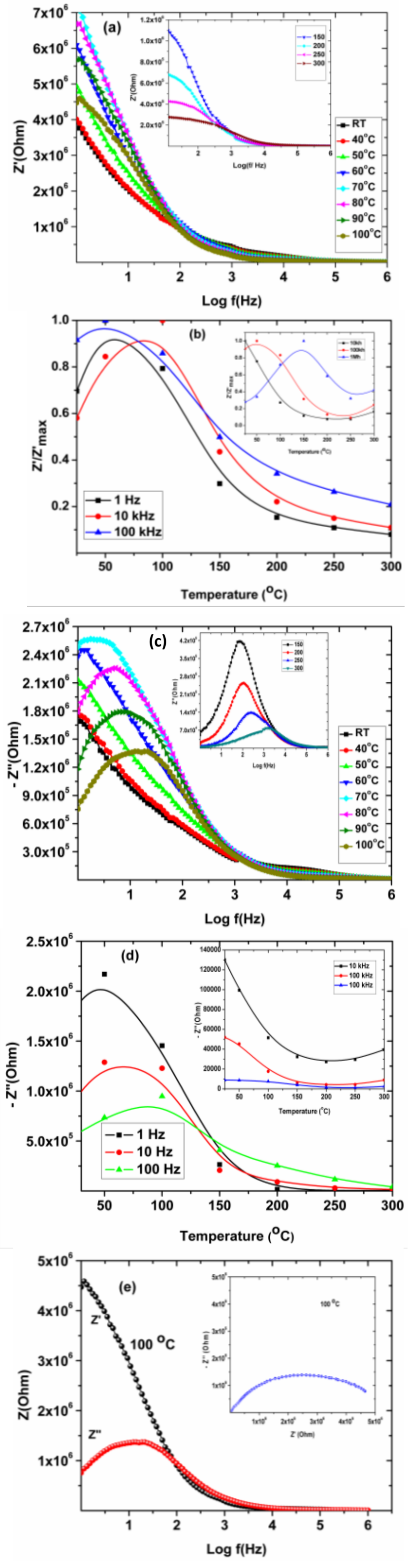

Fig. 2. (a) and (b) Variation of the real part of impedance with respect to frequency at various temperatures; (c) and (d) variation of the imaginary part of impedance with respect to frequency at various temperatures; and (e) frequency dependence of Z’ and Z” at 373 K.

The EDAX spectrum of the LiFeO$_2$ sample is shown in **Fig. 1(b)** and the SEM image is shown as an inset of **Fig. 1(b)**. The EDAX spectrum displays the characteristic peaks corresponding to the binding energy state of iron and oxygen. The peak positions identified are Fe K_α, Fe L_β and O $K_{\alpha 1.}$ No other impurity peaks are detected in the spectrum, which is an indication of the chemical purity of the sample. Lithium binding energy state can not be possible to detect from EDAX data for the obvious reason that the X-ray fluorescence yield is extremely low for Li. The estimation Fe to O ratio (Fe/O) value is obtained the 0.52. The SEM analysis revealed that the sample consists of homogeneously distributed cubical shaped micro-crystals with an average grain size of about 500 nm.

Electrical analysis

The response of the real components of impedance (Z’) with frequency for the LiFeO$_2$ sample at different temperatures is shown in **Fig. 2(a)** and **(b)**. Figure shows three regions for all temperatures: At higher frequency > 10^3 and at low frequencies < 10 Hz. At higher frequencies > 10^3 Hz, Z’ is almost independent of frequency, which is attributed to the resistance effect. In the frequency range between these limits, Z’ considerably decreases as the frequency increases. This indicates that the components of capacity and resistance of the equivalent circuit are active in this range of frequencies. However, for the frequencies < 10^3 Hz, Z’ decreases as temperature increases, implying a decrease in the total resistance of the LiFeO$_2$ sample. The real component of impedance (Z’) is gradually decreased as the temperature increases. The normalized Z’ is observed to shift slightly towards higher temperature region as frequency increases.

Fig. 2(c) and **(d)** show the variation of the imaginary component of the impedance (Z”) with the frequency for different temperature of LiFeO$_2$. The Figure shows relaxation or Debye-type peaks in the low frequency region and the peak intensity and peak shift towards higher frequency region as temperature increases. The increase in the imaginary component of the impedance (Z”) indicates that the total resistance of the sample is decreases whereas the shift indicates increasing of relaxation time (τ), loss in the material. The Z''_{max} values are proportional to grain resistance (R_g) given by the relation $Z'' = R_g[\omega\tau/(1 + (\omega\tau)^2)]$. The τ value has been calculated from the peak of Z” and the asymmetric broadening of the peak suggest the spread of τ at a temperature. If ‘τ’ increase, the relaxation process become slower and vice versa. From the **Fig. 2(e)**, it is observed that the Z’ as well as Z” curves merges above 100 kHz for all temperatures. This may be due to the reduction of the space charge effect. The contribution of the impedance from the grain predominates over the grain boundary at higher frequencies [**21**]. **Fig. 3** shows the Cole-Cole plots of LiFeO$_2$ sample with different temperature. These plots allow the resistances related to grain interiors (bulk), grain boundaries and sample/electrode interfaces to be separated because each of them has different relaxation times, resulting in separate semicircles in the complex impedance plane. The relaxation frequency for the bulk is one or two orders of magnitude higher than the relaxation frequency for grain boundaries and the relaxation frequency resulting from the electrode process is much smaller than relaxation frequency of grain boundaries [**22**].

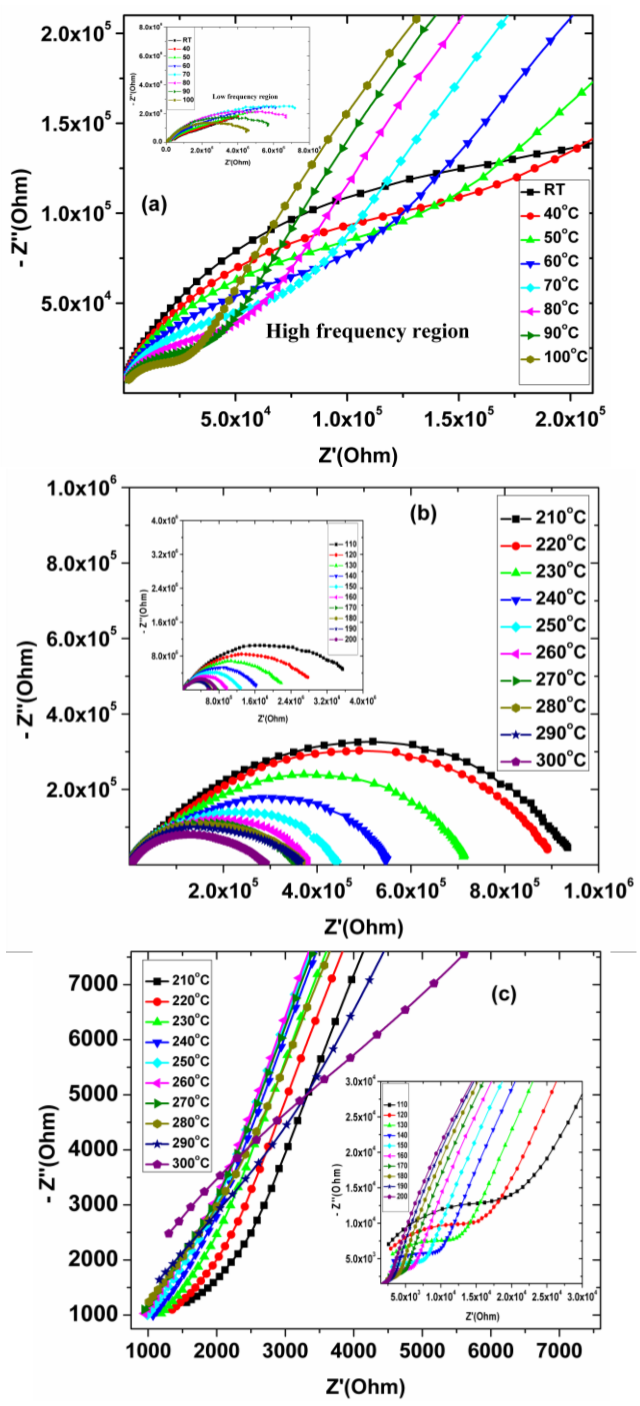

Fig. 3. (a), (b) and (c) Cole-Cole plots of LiFeO$_2$ at various temperatures.

In **Fig. 3**, the complex plane of LiFeO$_2$ sample, there are two regions for all temperature, which indicates different polarization mechanisms within the sample. At higher frequencies, the figure shows the semicircular arc, which is attributed to the electrical properties of a parallel combination of bulk resistance and capacitance of the LiFeO$_2$ sample. At intermediate and low frequencies, the complex impedance plots for all temperatures show two overlapped semicircular arcs, which are attributed to the distribution of the grain boundary and the sample/electrode interfaces of the $LiFeO_2$. However, the overlapping of the grain boundary and sample/electrode interfaces semicircles is more visible at higher temperatures. The radii of the bulk, grain boundary and sample/electrode interface semi circles decreases as temperature increases from room temperature to 573 K, which indicates decrease in the total resistance of the sample and this explains the decrease of Z' and Z" as shown in **Fig. 2(a)** and **Fig. 2(d)** [**23**]. The decrement in the grain and grain boundary resistance is attributed to the conduction mechanism at the grain – grain boundary.

The bulk conductivity (σ) value has been calculated using the formula [**24**],

$$\sigma = L/R_bA \text{ S m}^{-1} \qquad (7)$$

where, R_b is bulk resistance of the sample, L is the thickness of the pellet, A is the effective area.

The conductivity values are calculated from the above relation and it is observed that the ionic conductivity increases with respect to temperature and it has been found to be 1.9 x 10^{-6} S/m at 373 K.

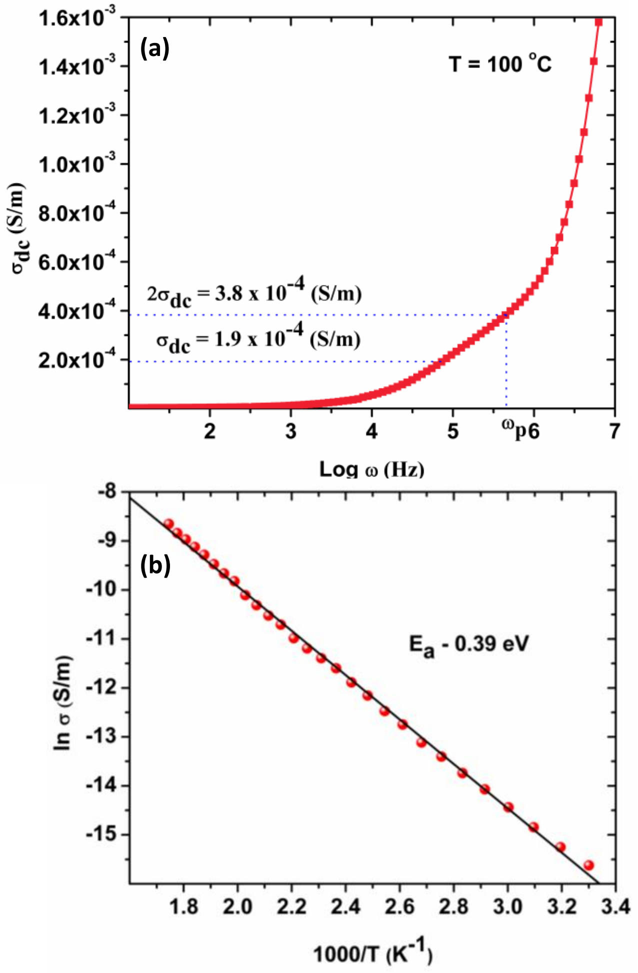

Fig. 4. (a) Graph between 'σ' versus log(ω) at 373 K. (b). Log (σ) versus 1000/T of $LiFeO_2$ sample.

Fig. 4 represents the graph $\sigma(\omega)$ versus log ω for $LiFeO_2$ sample at 373 K. The figure clearly show two distinct regions; a low frequency plateau indicating the dc conductivity of the material and high frequency dispersion region which obeys the power law feature $\sigma(\omega)$ proportional to ω^s. The material obeys the Jonsher's universal power law equation given by-

$$\sigma_{ac} = \sigma_0 + A\omega^s \qquad (8)$$

where σ_0 is the conductivity at zero frequency, which is normally called the dc conductivity, A is a constant, and s is a characteristic parameter (0<s<1).

In the figure, it can be seen that there is a plateau the low-frequency region and extrapolating it on the Y-axis gives the value of d.c. conductivity. Almond and West [**25**] have proposed that the $\sigma(\omega)$ data can be used to estimate the ionic hopping rate, ω_p. Extrapolating at twice the value of d.c conductivity from the vertical axis horizontally towards the graph and then extrapolating downwards vertically to the horizontal axis will give ω_p as shown in **Fig. 4(a)**. The hopping rate of ions, ω_p can also be given by the following relation:

$$\omega_p = \sigma T/K \qquad (9)$$

where $K = ne^2 a^2 \gamma k^{-1}$. Here, T is the temperature in Kelvin, K is charge carrier concentration term, e is electron charge, γ is correlation factor which is set equal to 1, and a is the distance between two adjacent sites for the ions to hop. a is taken as 3 Å based on the literature [**26**]. The density of charge carriers, n, the ionic mobility, μ, and diffusion coefficient, D, were calculated using following equations and are given in **Table 1**.

$$\mu = \sigma/ne \qquad (10)$$

$$D = kT\sigma/ne \qquad (11)$$

Table 1. Varies physical properties of $LiFeO_2$.

T (°C)	σ x 10^{-5} (S/m)	ω_p (Hz)	K x 10^{-7} ($S m^{-1} K Hz^{-1}$)	n x 10^{26} (m^{-3})	μ x 10^{-13} ($m^2 V^{-1} s^{-1}$)	D x 10^{-15} ($m^3 s^{-1}$)
RT	2.96	38467	2.10	12.58	1.47	3.46
40	3.10	47626	2.03	12.19	1.59	4.28
50	4.39	95705	1.48	8.87	3.09	8.6
60	5.53	126528	1.45	8.71	3.96	11.38
70	9.52	292344	1.11	6.68	8.89	26.31
80	1.21	336131	1.27	7.63	9.94	30.25
90	1.51	386484	1.41	8.49	10.10	34.78
100	1.90	444373	1.59	9.53	12.40	39.99

It is observed from the Table that there is no significant variation in K and n within the temperature range studied. So it can be concluded that the conduction mechanism in $LiFeO_2$ is attributed to the hopping of charge carriers. The ionic mobility (μ) is observed to be increased with increase in temperature and this suggest that the conductivity of the $LiFeO_2$ sample can be attributed to enhance in ionic mobility since number density of the mobile ions is considered to be constant. The diffusion coefficient (D) is also observed to be increased from 3.46 x 10^{-15} m^3/s to 3.99 x 10^{-14} m^3/s with increase in temperature.

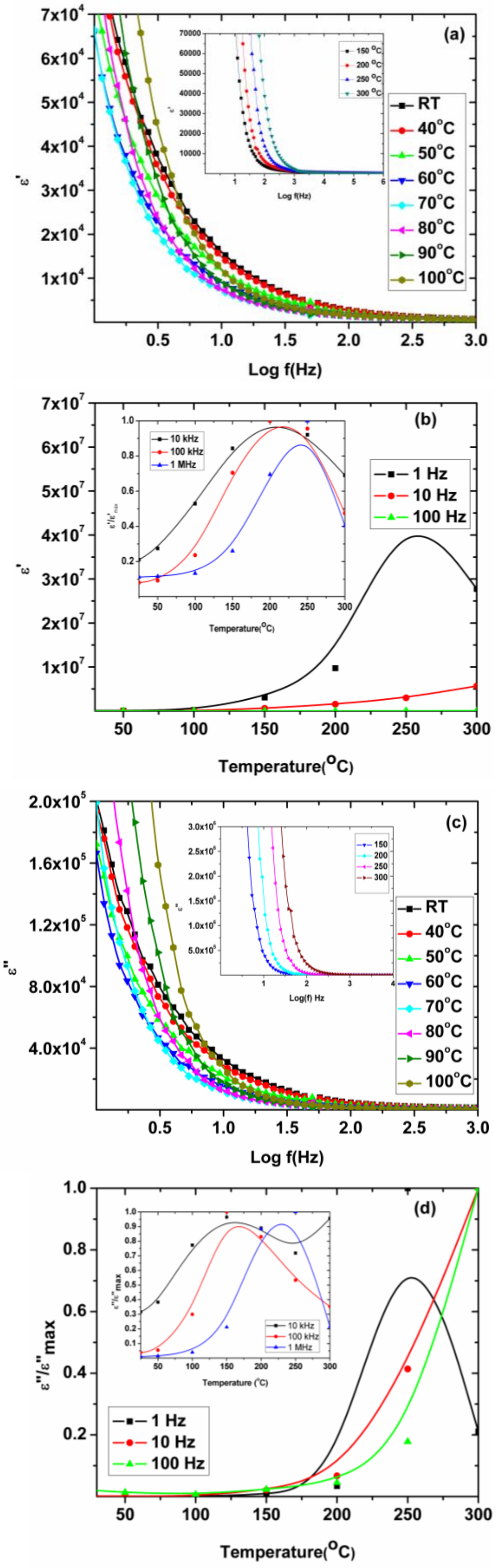

Fig. 5. (a) and (b) Variation of the real part of dielectric constant with respect to frequency at various temperatures; (c) and (d) Variation of the imaginary part of dielectric constant with respect to frequency at various temperatures.

Fig. 4(b) shows the temperature dependence of conductivity for $LiFeO_2$ sample. From the plot of ln σ versus 1000/T for $LiFeO_2$ sample, the temperature dependence of ionic conductivity obeys Arrhenius rule:

$$\sigma = \sigma_o \exp(-E_a/kT) \qquad (12)$$

Where σ_o is a pre-exponential factor, E_a is the activation energy of conduction, T is temperature in Kelvin and k is Boltzmann constant. From the slope of the graph, activation energy can calculate. The estimated activation energy for $LiFeO_2$ is 0.39 eV [**27**]. It is observed that the conductivity increases linearly with temperature gives that the conduction is thermally activated process.

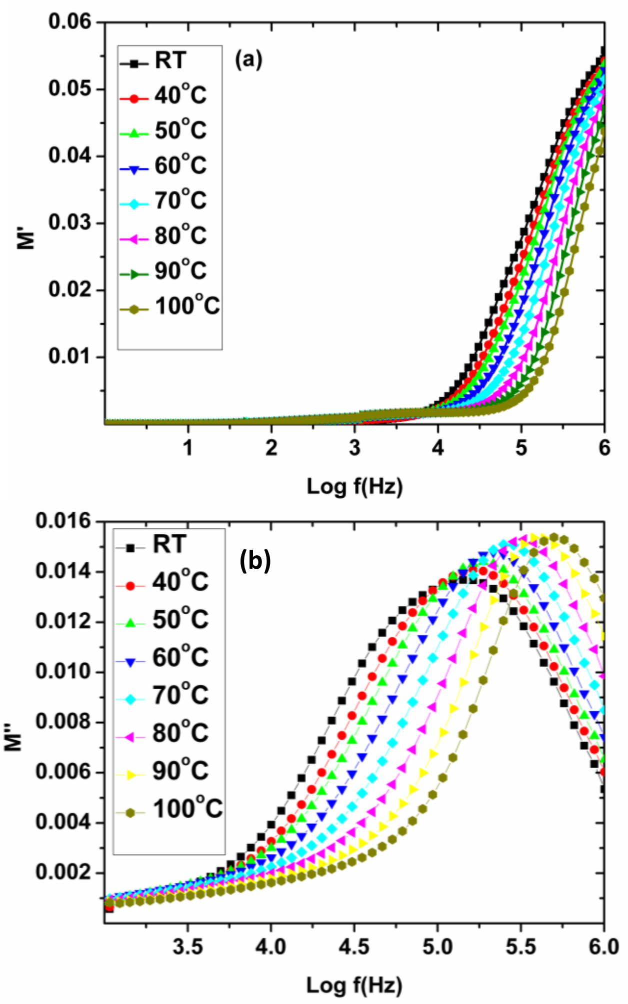

Fig. 6. (a) and (b) Variation of real and imaginary part of modulus of $LiFeO_2$ at various temperatures.

Dielectric studies

The real part of the dielectric permittivity or dielectric constant, ε' and imaginary part of dielectric permittivity or dielectric loss, ε'', for $LiFeO_2$ sample measured in the frequency range 1 Hz to 1 MHz various temperatures is shown in **Fig. 5(a)** and **(b)**. It is observed that the dielectric constant, ε'(ω) is decreased rapidly at lower frequencies and showed almost frequency independent behavior at higher frequency region[**28**]. The bulk polarization of the sample results from the presence of electrodes, which do not allow transfer of the charge species into the external circuit. At higher temperatures, $\varepsilon'(\omega)$ is observed to be increased and it might be due to migration of the lithium ion. The behavior of the dielectric permittivity with frequency is related to the applied field, which assists electron hopping between two different sites of the sample. At higher frequency region, the charge carriers will no longer be able to rotate sufficiently rapidly, so their oscillation will begin to lay behind this field resulting in a decrease of dielectric permittivity, $\varepsilon'(\omega)$. Generally, the relaxation phenomena in dielectric materials are associated with frequency dependent orientational polarization. At low frequency region, the permanent dipoles align themselves along the field and contribute fully to the total polarization of the dielectric. At higher frequency region, the variation in the field is very rapid for the dipoles to align themselves, so their contribution to the polarization and hence, to dielectric permittivity can become negligible. Therefore, the dielectric permittivity, $\varepsilon'(\omega)$ decreases with increasing frequency. The decrease of the dielectric constant ε' can also explain from interfacial polarization. The interfacial polarization arises as a result of difference in conducting phase, but is interrupted at grain boundary due to lower conductivity. Generally in polycrystalline materials, the grains exhibits semi conducting behavior while the grain boundary are insulators.

The frequency dependence of the dielectric loss, $\varepsilon''(\omega)$ at different temperatures is shown in **Fig. 5(c)**. The maximum in the $\varepsilon''(\omega)$ peak is shifts towards higher frequency region as the temperature increase indicating a thermally activated behavior. Generally, the dielectric losses at high frequencies are much lower than those occurring at lower frequencies at specific temperature. This kind of dependence of $\varepsilon''(\omega)$ on frequency is typically associated with losses by conduction.

An alternate approach to analyze electrical relaxation is electric modulus. The electric modulus M^* can be defined in terms of the reciprocal of the complex dielectric constant $\varepsilon^*(\omega)$ as,

$$M^* = 1/\varepsilon^*(\omega) = M'(\omega) + M''(\omega) \qquad (13)$$

where real part of complex modulus M' and imaginary part of complex modulus M'' can be calculated by using equations (5) and (6).

The frequency dependence of $M'(\omega)$ and $M''(\omega)$ of $LiFeO_2$ at different temperatures is shown in **Fig. 6**. These Figures explain the relaxation nature of dielectric properties of the sample. The $M'(\omega)$ is increases with temperature and the maximum in the $M''(\omega)$ shifts towards higher frequency region with increasing temperature [**29**]. The frequency above peak maximum $M''(\omega)$ determines the range in which charge carriers are mobile on long distances. At frequency above peak maximum $M''(\omega)$, the carriers are spatially confined to potential wells, being mobile on short distances making only localized motion within the wells. The relaxation time, τ also calculated from the $M''(\omega)$ peak by using the following relation, $\tau = 1/\omega_{peak}$ and is observed to decrease with increasing temperature as shown in **Fig. 7**.

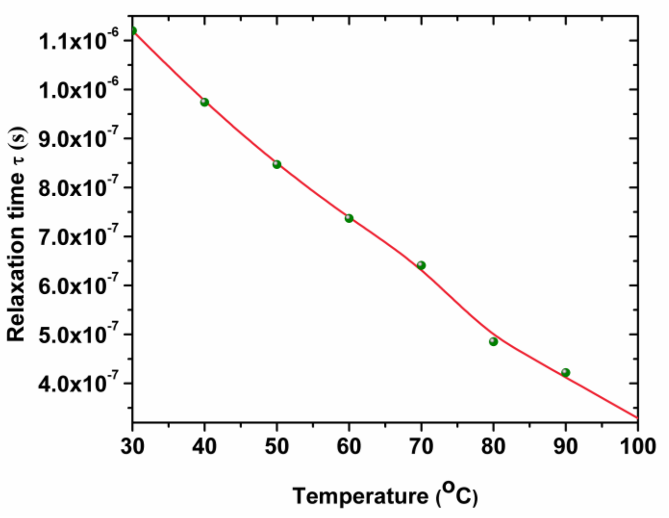

Fig. 7. Relaxation time (τ) versus temperature.

Conclusion

$LiFeO_2$ cathode material was synthesized by hydrothermal method. The X-ray diffraction pattern of the prepared powder was conformed the formation of α-$LiFeO_2$ with face centered cubic rock salt structure. The estimated particle size of the $LiFeO_2$ from SEM studies is about 500 nm. The plot of log conductivity against reciprocal temperature obeys Arrhenius rule. Transport parameters such as activation energy, ionic hopping frequency, carrier concentration, ionic mobility and diffusion coefficient have been calculated. The activation energy calculated from the Arrhenius plots was found to be 0.39 eV. The dielectric constant was observed to decrease with increase in frequency. The variation of M'' as a function of frequency shows the shifting of the peaks towards the high frequency as temperature increases which implies that there is a distribution of ionic relaxation time. The ionic conductivity of the sample was found to be varied from 2.95×10^{-7} S/m to 1.74×10^{-4} S/m by increase in temperature from room temperature to 573 K.

Acknowledgements
Authors would like to thank University Grants Commission, New Delhi for providing financial assistance.

References:

1. Jeevan Kumar, P.; Jayanth Babu, K.; Hussain, O.M. Adv. Sci. Eng. Med. **2012**, 4, 190.
   DOI: 10.1166/asem.2012.1147
2. Sheu, S.P.; Shih, I.C.; Yao, C.Y.; Chen, J.M.; Hurng, W.M. J. Power Sources **1997**, 68, 558.
   DOI: 10.1016/S0378-7753(97)02526-3
3. Jinhan Yao.; ChaoqiShen.; PinjieZhang.; Duncan Gregory, H.; Lianbang Wang. J. Phys. Chem. Solids **2012**, 73, 1390.
   DOI: 10.1016/j.jpcs.2012.07.006
4. Lee, Y.S.; Sato, S.; Sun, Y.K.; Kobayakawa, K.; Sato, Y. J. Power Sources **2003**, 119, 258.
   DOI: 10.1016/S0378-7753(03)00152-6
5. Robert Armstrong, A.; Daniel Tee, W.; Fabio La Mantia.; Petr Nova, k.; Peter Bruce, G. J. Amer. Chem. Soc. **2008**, 130, 3554.
   DOI: 10.1021/ja077651g. ISSN: 0002-7863
6. Heike Gabrisch.; Yasunori Ozawa.; Rachid Yazami. Electrochimica Acta **2006**, 52 1499.
   DOI: 10.1016/j.electacta.2006.02.050
7. Abdel-Ghany, A.E.; Mauger, A.; Zaghib, H.; Julien, C.M. J. Power Sources **2012**, 197, 285.

DOI : 10.1016/j.powsour.2011.09.054

8. Lee, Y.S.; Sato, S.; Tabuchi, M.; Yoon, C.S.; Sun, Y.K.; Kobayakawa, K.; Sato, Y. Electrochem. Commun. **2003**, 5, 549.
   DOI: 10.1016/S1388-2481(03)00118-8
9. Masaaki Hirayama.; Hiroki Tomita.; Kei Kubota.; Ryoji Kanno.; J. Power Sources **2011**, 196, 6809.
   DOI: 10.1016/j.jpowsour.2010.10.009
10. Galakhov, V.R.; Kurmaev, E.Z.; Uhlenbrock, S. Solid State Commun. **1995**, 95, 347.
    DOI: 10.1016/0038-1098(95)00279-0
11. Michele Catti.; Merced Montero-Campillo.; J. Power Sources **2011**, 196, 3955.
    DOI: 10.1016/j.jpowsour.2010.11.062
12. Santos-Pena, J.; Crosinier, O.; Brousse, T. Electrochimica Acta **2010**, 55, 7511.
    DOI: 10.1016/j.electacta.2009.12.069
13. Lee, Y.S.; Sato, S.; Tabuchi, M. Electrochem. Commun. **2003**, 5, 549.
    DOI: 10.1016/S1388-2481(03)00118-8
14. Ashutosh Tiwar.; Ajay Mishra, K.; Hisatoshi Kobayashi.; Anthony Turner, P.F. Wiley, USA, ISBN 978-04-709387-99, **2012**.
15. Jingwen Yao.; Feng Wu.; Xinping Qiu.; Ning Li.; Yuefeng Su. Electrochimica Acta **2011**, 56, 5587.
    DOI: 10.1016/j.electacta.2011.03.141
16. Prabu, M.; Selvasekarapandian, S.; Kulkarni, A.R.; Hirankumar , G.; Sanjeeviraja, C. J. Rare Earths **2010**, 28, 435.
    DOI: 10.1016/S1002-0721(09)60128-9
17. Prabu, M.; Selvasekarapandian, S.; Kulkarni, A. R; Hirankumar, G.; Sakunthala. A. Solid State Ionics **2010**, 16, 317.
    DOI : 10.1007/s11581-010-0420-7
18. Sung-Woo Kim,.; Su-Il Pyun. J. Electroanalytical. Chem. **2002**, 528, 114.
    DOI: S0022-0728(02)00900-2
19. Vijayakumar, M.; Selvasekarapandian, S.; Kesavamoorthy, R.; Koichi Nakamura.; Tatsuo Kanashiro. Mater. Lett. **2003**, 57, 3618.
    DOI: 10.1016/S0167-577X(03)00137-X
20. Julian Morales.; Jesus Santos-Pena. Electrochem. Commun. **2007**, 9, 2116.
    DOI: 10.1016/j.elecom.2007.06.013
21. Rao, K.S.; Krishna, P.M.; Prasad, D.M.; Latha, T.S.; Hussain, M. Euro. Phys. J. Appl. Phys. **2007**, 39, 24.
    DOI: 10.1051/epjap:2007125
22. Prakash, D.; Yoshitake Masuda.; Sanjeeviraja, C. Solid State Ionics **2012**, 18, 35.
    DOI : 10.1007/s11581-011-0595-6
23. Subrat, K.; Barik.; Choudhary, R.N.P.; Singh, A.K. Adv. Mat. Lett. **2011,** 2, 419.
    DOI: 10.5185/amlett.2011.2228
24. Jonscher, A.K. Dielectric relaxation in solids (Chelsea Press, London, 1983).
25. Almond, DP.; West, AR. Solid State Ionics **1987**, 23, 27.
    DOI: 10.1016/0167-2738(87)90078-6
26. Vijayakumar, M.; Hirankumar, G.; Bhuvaneswari, M.S.; Selvasekarapandian, S. J. Power Sources **2003**, 117, 143.
    DOI: 10.1016/S0378-7753(03)00110-1
27. Sohn, R S T M.; Macedo, A A M.; Costa, M M.; Mazzetto, S E.; Sombra, A S B. Physica Scripta, **2010**, 82, 6.
    DOI: 10.1088/0031-8949/82/05/055702
28. Chandra babu, B.; Naresh, V.; Jaya Prakash, B.; Buddhudu, S. Ferroelectrics Lett. **2011**, 38, 124.
    DOI: 10.1080/07315171.2011.623610
29. Louati, B.; Guindara, K. Mater. Sci. Eng. B **2012**, 117, 838.
    DOI: 10.1016/j.mseb.2012.03.050